

Elemental Abundance Measurements in Low-redshift Damped Lyman- α Absorbers

Joseph D. Meiring¹, Varsha P. Kulkarni¹, Pushpa Khare², Jill Bechtold³, Donald G. York^{4,5}, Jun Cui³, James T. Lauroesch⁶, Arlin P. S. Crotts⁷, Osamu Nakamura⁸

¹*Department of Physics and Astronomy, University of South Carolina, Columbia, SC 29208, USA*

²*Department of Physics, Utkal University, Bhubaneswar, 751004, India*

³*Department of Astronomy and Astrophysics, University of Arizona, Tucson, AZ 85721, USA*

⁴*Department of Astronomy and Astrophysics, University of Chicago, Chicago, IL 60637, USA*

⁵*Enrico Fermi Institute, University of Chicago, Chicago, IL 60637, USA*

⁶*Department of Physics and Astronomy, Northwestern University, Evanston, IL 60208, USA*

⁷*Department of Astronomy, Columbia University, New York, NY 10027, USA*

⁸*School of Physics and Astronomy, University of Nottingham, NG7 2RD, UK*

Accepted ... Received ...; in original form ...

ABSTRACT

We present elemental abundance measurements for 9 damped Ly- α systems (DLAs) and 1 sub-DLA at $0.1 \lesssim z \lesssim 1.5$ from recent observations with the Multiple Mirror Telescope. Most of these absorbers are found to be metal-poor, while 2 are found to have $\approx 30 - 50\%$ solar metallicities. Combining our data with other data from the literature, we find that the systems with higher $[\text{Zn}/\text{H}]$ also have stronger depletion as measured by $[\text{Cr}/\text{Zn}]$ and $[\text{Fe}/\text{Zn}]$. The relationship between the metallicity and H I column density is also investigated. Together with our previous MMT survey (Khare et al. 2004) we have discovered 2 of the 4 known absorbers at $z < 1.5$ that lie above (although near) the “obscuration threshold”. This appears to be a result of selecting absorbers with strong metal lines in our sample. It would be interesting to find other similar systems by observing a larger sample and study how much such systems contribute to the cosmic budget of metals. Finally, an analysis of the N_{HI} -weighted mean metallicity vs. redshift for our sample combined with data from the literature supports previous conclusions that the N_{HI} -weighted mean global DLA metallicity rises slowly at best and falls short of solar levels by a factor of > 4 even at $z = 0$.

Key words: Quasars: absorption lines-ISM: abundances, dust, extinction

1 INTRODUCTION

Absorption line systems in QSO spectra provide a unique window into the high-redshift universe. These systems have been detected in the range $0 \lesssim z \lesssim 6$, corresponding to $\sim 90\%$ of the age of the universe. As the absorption line strengths depend primarily on the gas content, they are selected independent of the stellar luminosities of the galaxies. Thus in principle they may be expected to provide less biased probes of galaxies than objects used to study the high redshift universe through emission, which are biased toward brighter galaxies including actively star forming galaxies such as Lyman-break galaxies, active galaxy nuclei, and QSOs.

Damped Lyman- α Absorption systems (DLAs) with $\log N_{\text{HI}} \geq 20.3$ and sub-DLAs with $19.0 \leq \log N_{\text{HI}} < 20.3$ seen in QSO spectra can be used as probes of the neutral gas content of the universe. DLAs and sub-DLAs are known to contain the majority of the neutral gas in the universe (e.g. Wolfe et al. 1995, Peroux et al. 2003). With such high neutral hydrogen column densities DLAs are believed to be closely linked to galaxies. DLAs may also be the

neutral gas reservoirs used in star formation. Furthermore, DLAs and sub-DLAs provide detailed gas-phase abundances of a number of elements and can thus be used to test galactic chemical evolution models.

Several elements have been detected in DLAs including C, N, O, Mg, Si, S, Ca, Ti, Cr, Mn, Fe, Ni, and Zn. Zn is often used as a tracer of gas-phase metallicity as it is typically relatively undepleted in the Galactic ISM when the fraction of H in molecular form is low, which is the case for DLAs (Sembach et al. 1995), Zn tracks the abundance of Fe in Galactic stars (Mishenina et al. 2002), and the lines of Zn II $\lambda\lambda$ 2026,2062 are fairly weak and unsaturated. Also, Zn II can be detected with ground-based observations over a wide range of redshifts ($0.6 \lesssim z \lesssim 3.5$). Elemental abundances relative to Zn such as $[\text{Cr}/\text{Zn}]$ or $[\text{Fe}/\text{Zn}]$ can be used to estimate the dust content of the QSO absorber. Here and throughout the paper we adopt the standard notation $[\text{X}/\text{H}] = \log(N_{\text{X}}/N_{\text{HI}}) - \log(\text{X}/\text{H})_{\odot}$.

If DLAs do constitute a representative sample of galaxies, it would be expected that their global mean metallicity of these ob-

jects should rise to roughly solar values at low redshift. It is uncertain whether or not DLAs show this trend. The most recent evaluations of this by Kulkarni and Fall (2002), Prochaska et al. (2003b), and Kulkarni et al. (2005) show at best a weak evolution in the metallicity-redshift relation with slopes of $\sim -0.20 \pm 0.07$.

One proposed explanation of the lack of metal-rich DLAs in observed samples is that this population is being under-sampled due to dust obscuration (e.g.; Boisse et al. 1998; Pei & Fall 1993; Vladilo & Peroux 2005). Absorbers with higher metallicity may also contain more dust, making any background QSOs fainter and keeping those objects out of magnitude-limited samples (York et al. 2006). In fact, it has been claimed that up to 50 % of QSOs may be hidden in optical surveys due to dust obscuration (Vladilo & Peroux 2005). Recently, Akerman et al. (2005) measured the metal abundances of $z > 1.8$ DLAs from the Complete Optical and Radio Absorption Line System survey (CORALS), and found that N_{HI} weighted mean metallicity based on the Zn abundance is only marginally higher but within error limits of previous samples. However, the effects of dust may be expected to be stronger at low redshifts. The role of dust in DLAs is still unclear, and more investigation is needed. We discuss dust and reddening in our sample of absorbers in more detail in § 5.2.

Assuming a cosmology with $\Omega_m = 0.3$ and $\Omega_\Lambda = 0.7$, $z < 1.5$ spans ~ 70 % of the age of the universe. It is therefore critical to obtain more abundance measurements at low redshift. One reason for the uncertainty in the metallicity-redshift relation is the lack of abundance measurements in low-redshift absorbers. In fact ~ 70 % of the existing Zn measurements are for $2 \lesssim z \lesssim 3.5$, which corresponds to only ~ 10 % of the age of the universe. The paucity of Zn measurements at low z is primarily because the Zn $\lambda\lambda$ 2026, 2062 lines lie in the UV for $z < 0.6$, and deeply in the blue end of the spectrum for $0.6 < z \lesssim 1.3$, where most existing spectrographs are inefficient. In this paper we present new MMT observations toward 10 QSOs. The observations presented in this paper increases the size of the sample of absorbers at $z \lesssim 1.5$ by ~ 40 %.

In § 2 we describe our observations and our data reduction routines. § 3 describes the estimation of column densities. In § 4 we present notes on the individual objects. We present results from these measurements in § 5, and in § 6 we discuss our results and their implications.

2 OBSERVATIONS AND DATA REDUCTION

Our sample consists of 10 confirmed DLA and sub-DLA absorbers at $0.2 \lesssim z \lesssim 1.5$, for which N_{HI} is known from *HST* spectra (Rao et al. 2005). Seven of these targets were observed in the Sloan Digital Sky Survey (SDSS), and most show the presence of strong Mg II or Fe II absorption features from SDSS spectra. Apparent magnitudes for these 7 QSOs are available from the SDSS Quasar Catalog III, Data release 3 (Abazajian et al. 2005).

The spectra presented here were obtained at the Multiple Mirror Telescope (MMT) during two separate epochs, 2004 May and 2005 February. Nearly 2.7 nights out of a total of 5 were lost due to poor weather. The Blue Channel spectrograph was used with the 832 l mm^{-1} grating in the first order, or the 1200 l mm^{-1} grating in the second order, depending on the redshift of the absorber. A CuSO_4 blocking filter was used with the 832 l mm^{-1} grating to block first order red light. The central wavelength for the 832 l mm^{-1} grating was at 3670 Å and 3600 Å for the 2004 May and 2005 Feb epochs respectively. For the 1200 l mm^{-1} grating the wavelength was centered at 4935 Å and 4770 Å during the 2004 May and 2005 Feb

Table 1. Atomic Data

Species	λ_{rest} Å	f	References
Be II	3130.4219	3.321E-1	1
C IV	1548.2040	1.899E-1	1
	1550.7810	9.475E-2	1
Mg I	1827.9351	2.420E-2	1
	2026.4768	1.130E-1	1
	2852.9631	1.830E00	1
Mg II	2796.3543	6.155E-1	1
	2803.5315	3.058E-1	1
Al II	1670.7886	1.710E00	1
Al III	1854.7184	5.590E-1	1
	1862.7910	2.780E-1	1
Si II	1808.0129	2.080E-3	1,2
Si IV	1393.7602	5.130E-1	1
	1402.7729	2.540E-1	1
Ca II	3933.6614	6.267E-1	1
	3968.4673	3.116E-1	1
Ti II	1910.6123	1.040E-1	1,3
	3383.7588	3.580E-1	1
Cr II	2056.2569	1.030E-1	1,2
	2062.2361	7.590E-2	1,2
Mn II	2576.8770	3.610E-1	1
	2594.4990	2.800E-1	1
	2606.4620	1.980E-1	1
Fe II	2249.8768	1.820E-3	4
	2260.7805	2.440E-3	4
	2344.2139	1.140E-1	1,5
	2374.4612	3.130E-2	1
	2382.7652	3.200E-1	1,5
Zn II	2026.1370	5.010E-1	1,6
	2062.6604	2.460E-1	1,6

References. (1) Morton 2003; (2) Bergeson & Lawler 1993b; (3) Wiese et al. 1996; (4) Bergeson et al. 1994; (5) Bergeson et al. 1996; (6) Bergeson & Lawler 1993a

epochs respectively. In order to achieve the desired S/N while minimizing cosmic rays, multiple exposures of each target were taken with exposure times ranging from 1800 to 2700 s depending on the magnitude of the QSO. Each target observation was followed by a comparison spectrum from a He+Ne+Ar lamp for wavelength calibration. Quartz flat fields and bias frames were taken at both the beginning and end of the night. Table 1 lists the vacuum wavelengths and oscillator strengths used in identification of the features and subsequent analysis. Table 2 gives a summary of our observations.

Data reduction was carried out using standard IRAF routines. Images were bias subtracted, trimmed, and flat fielded using the task CCDPROC. These reduced 2-d spectra were then extracted and wavelength calibrated using the task DOSLIT. The wavelengths were converted to vacuum using the task DISPTANS. Finally the spectrum was normalized using the task CONINUUM. The solar abundances used as reference while calculating the abundances are adopted from Lodders et al. (2003).

Figures 1-10 plot the co-added and continuum-fitted spectra obtained with the MMT, along with line identifications from the DLAs as well as other absorption systems along the line of sight. Unmarked, minor depressions have been verified to be artifacts.

Table 2. Summary of Observations

QSO	g	z_{em}	z_{DLA}	$\log N_{\text{HI}}$ cm^{-2}	Grating lines mm^{-1}	FWHM \AA	Exposure Time	Epoch
0738+313	16.1	0.630	0.0912	21.18 ± 0.06	832	1.10	3000	2005 Feb.
...	0.2210	20.90 ± 0.09	832	1.10	3000	2005 Feb.
0827+243	17.3	0.941	0.5247	20.30 ± 0.05	832	1.10	3600	2005 Feb.
1010+0003	18.3	1.398	1.2651	21.52 ± 0.07	1200	1.33	3600	2005 Feb.
1107+0003	18.7	1.741	0.9547	20.26 ± 0.14	832	1.10	8100	2005 Feb.
1137+3907	17.4	1.023	0.7190	21.10 ± 0.10	832	1.10	5400	2004 May
1225+0035	18.9	1.226	0.7731	21.38 ± 0.11	832	1.10	5400	2005 Feb.
1501+0019	18.1	1.930	1.4832	20.85 ± 0.13	1200	1.33	5400	2004 May
1712+5559	18.7	1.356	1.2095	20.72 ± 0.05	1200	1.33	5400	2004 May
1715+4606	18.1	0.989	0.6511	20.44 ± 0.13	832	1.10	5400	2004 May
1733+5533	18.1	1.074	0.9981	20.70 ± 0.03	832	1.10	3600	2004 May

3 ESTIMATION OF COLUMN DENSITIES

Column densities were estimated by fitting the observed absorption line profiles using the package FITS6P (Welty et al. 1991), which has evolved from the code by Vidal-Madjar et al (1977). FITS6P iteratively minimizes the χ^2 value between the data and a theoretical Voigt profile that is convolved with the instrumental profile. All lines were fit with a single component Voigt profile. If a multiplet was available such as Fe II $\lambda\lambda$ 2344, 2374, 2382 the lines were fit simultaneously until convergence for a common N , b_{eff} , and v . Equivalent width measurements were obtained with the package SPECP, also written by D.E. Welty. The 1σ equivalent width uncertainties were estimated using the photon noise uncertainties and the continuum uncertainties obtained by allowing the continuum to vary by $\pm 10\%$. In all cases these uncertainties were dominated by the photon noise uncertainties.

The prescription of Khare et al. (2004) for fitting the Cr II and Zn II lines of was followed. Specifically, the Cr II $\lambda\lambda$ 2056, 2066 lines were fit simultaneously to obtain N , b_{eff} , and v values. Then, the blended Cr II+Zn II λ 2062 line was fit starting with the values obtained from the previous fits, holding the Cr II component fixed. The Zn II λ 2026 line was then fit using the b_{eff} and v value from the Cr $\lambda\lambda$ 2056, 2062 fit while holding the Mg I component fixed. If the Cr II λ 2056 line could not be fit due to noise, we fit the Zn II λ 2026 line, holding the Mg I λ 2026 contribution fixed, then fit the Cr II + Zn II λ 2062 blend holding the Zn II component fixed. The Mg I column density was estimated by fitting the Mg I λ 2852 line from the SDSS spectra. York et al. (2006) showed that the Mg I λ 2852 lies on the linear portion of the curve of growth for $W_{\text{MgI}}^{\text{rest}} \sim 0.6$ to 0.7. The Mg I λ 2852 line is often moderately saturated in DLAs and the assumption of a linear curve of growth may lead to an underestimation of the Mg I column density, therefore we did not assume Mg I λ 2852 to be on the linear portion of the curve of growth, and instead used the results of a profile fit to that line. To judge the effects of possible saturation of Mg I λ 2852 on N_{MgI} and hence on N_{ZnII} , we also estimated the maximum N_{MgI} that would be consistent with W_{2852} within a 3σ level. We then used this maximum N_{MgI} to estimate the minimum N_{ZnII} in the λ 2026 line. In any case, in our experience the contribution of Mg I to the blended λ 2026 line is typically small (eg. Peroux et al. 2006a). For Q1501+0019 we also have a constraint on N_{MgI} from the non-detection of the Mg I λ 1827 line which gives $\log N_{\text{MgI}} < 13.47$.

Tables 3 and 4 list the derived equivalent widths and column densities respectively. If a certain species was not detected, 3σ upper limits were placed on the equivalent widths and column densi-

ties based on the signal to noise ratio (S/N) in the region based on a 3 pixel resolution element. It was assumed that these lines lie on the linear portion of the curve of growth. As can be seen in figures 1-10, none of the detected Zn II or Cr II lines are saturated. In fact, none of the lines detected appear to show significant saturation even in those cases where the equivalent widths are large. This is likely due to the line profile being composed of multiple components that could not be resolved at the resolution of our data.

4 DISCUSSION OF INDIVIDUAL OBJECTS

Q0738 + 313 ($z_{em} = 0.630$, $z_{abs} = 0.0912$ for system A and $z_{abs} = 0.2210$ for system B): Both of the systems listed are DLAs. The Zn and Cr lines were studied by Kulkarni et al. (2005) using *HST* data. The $\lambda\lambda$ 3933,3969 lines of Ca II appear in both systems A and B. We also placed upper limits on Ti II λ 3383 of system B. As the background QSO is very bright ($g = 16.1$), we were able to obtain high S/N of ~ 100 in the region. This gives an upper limit of $\log(N_{\text{TiII}}/N_{\text{HI}}) < -9.42$, with $[\text{Ti}/\text{H}] < -2.32$. The feature located at $\sim 5070 \text{ \AA}$ is an artifact from bad pixels in the CCD.

Q0827 + 243 ($z_{em} = 0.941$, $z_{abs} = 0.259$ for system A and $z_{abs} = 0.5247$ for system B): The Zn and Cr lines of system B were studied in detail at lower wavelengths by Khare et al. (2004). The Fe II $\lambda\lambda$ 2249, 2260, 2344, 2374, 2382, 2586, 2600 lines were measured previously. Strong Mg II $\lambda\lambda$ 2796, 2803 and Mg I λ 2852 lines were present in system B in the new spectra. The Mg I λ 2852 line was fit first to estimate b_{eff} and v values, which were used when fitting the Mg II doublet. Due to the strong saturation of the Mg II $\lambda\lambda$ 2796, 2803 doublet we give the derived column density as a lower limit. We were able to place upper limits on Ti II λ 3383 of $[\text{Ti}/\text{H}] = -1.45$ at $S/N \sim 60$ in the region. The feature located at $\sim 5070 \text{ \AA}$ is again an artifact from bad pixels in the CCD.

Q1010 + 0003 ($z_{em} = 1.4007$, $z_{abs} = 1.2651$): The Cr II $\lambda\lambda$ 2056, 2062, 2066 lines, as well as the Zn II $\lambda\lambda$ 2026, 2062 lines were detected with S/N of ~ 30 . As all the lines were detected, the full prescription outlined in § 2 was followed. The Mg I contribution to the blended Zn II+Mg I λ 2026 line was estimated from the SDSS spectrum. The Mg I λ 2852 has an equivalent width of $W_{rest} = 404 \text{ m\AA}$. This line was fit using a single component model, yielding $\log N_{\text{MgI}} = 12.67 \pm 0.05$. This component was held fixed in Mg I λ 2026 while the Zn II and Cr II $\lambda\lambda$ 2026, 2056, 2062, 2066 lines were fit simultaneously giving $\log N_{\text{ZnII}} = 12.96$.

Table 3. Equivalent Widths

QSO	z_{abs}	Species	λ_{rest} Å	W_{rest} mÅ	QSO	z_{abs}	Species	λ_{rest} Å	W_{rest} mÅ	
0738+313 $z_{em} = 0.630$	0.0912:A	Ca II	3933	189±13	1501+0019 $z_{em} = 1.930$	1.4832:A	Mg I	2852	952 ^a	
		Ca II	3969	54±10			Al III	1854	334±17	
	0.2210:B	Ca II	3933	63±10			Al III	1862	216±18	
		Ca II	3969	35±10			Si II	1808	295±16	
0827+243 $z_{em} = 0.941$	0.2590:A	Ti II	3383	<14	1.8510:B	1.9260:C	Cr II	2056	105±16	
		Ca II	3933	<34			Cr II	2066	<26	
		Ca II	3969	<34			Zn II+Mg I	2026	231±21	
	0.5247:B	Ti II	3383	<33			Zn II+Cr II	2062	191±18	
		Mg I	2852	602±29			C IV	1548	154±18	
		Mg II	2796	2416±27			C IV	1550	116±18	
1010+0003 $z_{em} = 1.398$	1.2651:A	Mg II	2803	2316±28	1712+5559 $z_{em} = 1.356$	1.1590:A	C IV	1548	254±14	
		Ti II	3383	<30			C IV	1550	154±14	
		Mg I	2852	404 ^a			Al II	1670	88±11	
		Al III	1854	104±21			Cr II	2056	<33	
		Al III	1862	<46			Cr II	2066	<33	
		Cr II	2056	91±19			Fe II	2344	415±30	
		Cr II	2066	69±15			Fe II	2374	240±27	
	0.5252:A	Fe II	2249	144±26	1.2093:B	1.1590:A	Fe II	2382	592±32	
		Fe II	2260	184±26			Zn II+Mg I	2026	<33	
		Fe II	2344	564±28			Zn II+Cr II	2062	<33	
		Fe II	2374	543±35			Mg I	2852	367 ^a	
		Fe II	2382	715±30			Cr II	2056	<35	
		Zn II+Mg I	2026	233±23			Cr II	2066	<35	
		Zn II+Cr II	2062	181±22			Fe II	2344	973±33	
1107+0003 $z_{em} = 1.741$	0.9547:B	Mn II	2576	<30	1715+4606 $z_{em} = 0.989$	0.6544:A	Fe II	2374	723±31	
		Mn II	2594	<34			GAL ^b	Fe II	2382	1168±35
		Mn II	2606	<20				Zn II+Mg I	2026	<35
		Fe II	2344	139±36				Zn II+Cr II	2062	<35
		Fe II	2374	<47				Ca II	3933	1556±46 ^c
		Fe II	2382	269±36				Ca II	3969	205±36
		Fe II	2586	185±25				Cr II	2056	<165
	Fe II	2600	342±27	Cr II	2066	<165				
	1.711:C	Ti II	1910	<42	1733+5533 $z_{em} = 1.074$	GAL ^b	Fe II	2344	1264±42	
		Cr II	2056	<27			Fe II	2374	851±40	
		Cr II	2066	<27			Fe II	2382	1556±46 ^c	
		Zn II+Mg I	2026	<27			Zn II+Mg I	2026	<165	
		Zn II+Cr II	2062	<27			Zn II+Cr II	2062	<165	
		Si IV	1393	618±36			Ca II	3933	482±36	
Si IV		1402	447±40	Ca II			3969	257±33		
1137+3907 $z_{em} = 1.023$	GAL ^b	Ca II	3933	336±58	0.9984:A	1.1496:B	Mg I	2852	362 ^a	
		Ca II	3969	241±51			Al III	1854	179±31	
	0.7190:A	Cr II	2056	<74			Al III	1862	100±27	
		Cr II	2066	<74			Si II	1808	178±30	
		Fe II	2249	150±31			Ti II	1910	<30	
		Fe II	2260	291±34			Cr II	2056	<35	
		Fe II	2344	1768±67			Cr II	2066	<29	
		Fe II	2374	1300±37			Zn II+Mg I	2026	<29	
		Fe II	2382	2009±70			Zn II+Cr II	2062	<29	
	0.7731:A	Zn II+Mg I	2026	447±56			C IV	1548	453±55	
		Zn II+Cr II	2062	266±70			C IV	1550	341±51	
		Mg I	2852	929 ^a			Al II	1670	<40	
		Cr II	2056	259±81			Al III	1854	<30	
		Cr II	2066	177±76			Al III	1862	<30	
Fe II		2249	339±73	Si II	1808	<25				
Fe II		2260	372±80				
1225+0035 $z_{em} = 1.226$	Zn II+Mg I	2026	<122				
	Zn II+Cr II	2062	181±91				
				

^a: From SDSS spectra. ^b: Entries with GAL identifier are from lines originating in the Milky Way. ^c: The Galactic Ca II λ 3933 line and Fe II λ 2383 line from the DLA at $z_{abs} = 0.6544$ are blended in the spectra.

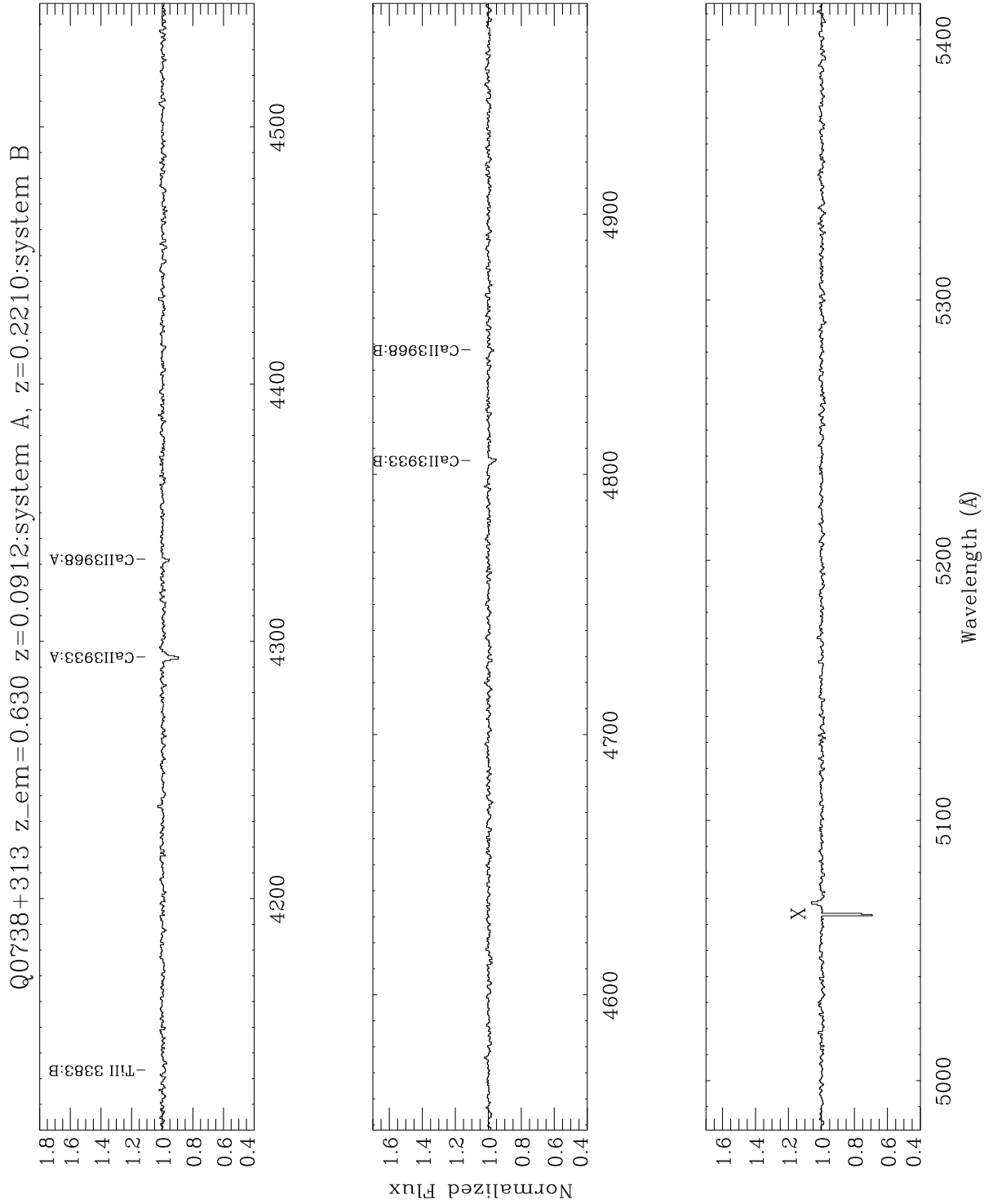


Figure 1. Combined and normalized spectrum of Q0738+313. The expected positions of several lines of interest are marked above the continuum with their rest wavelength and species. The letters after the wavelengths refer to the different systems indicated at the top of the figure. An “X” signifies a defect in the CCD.

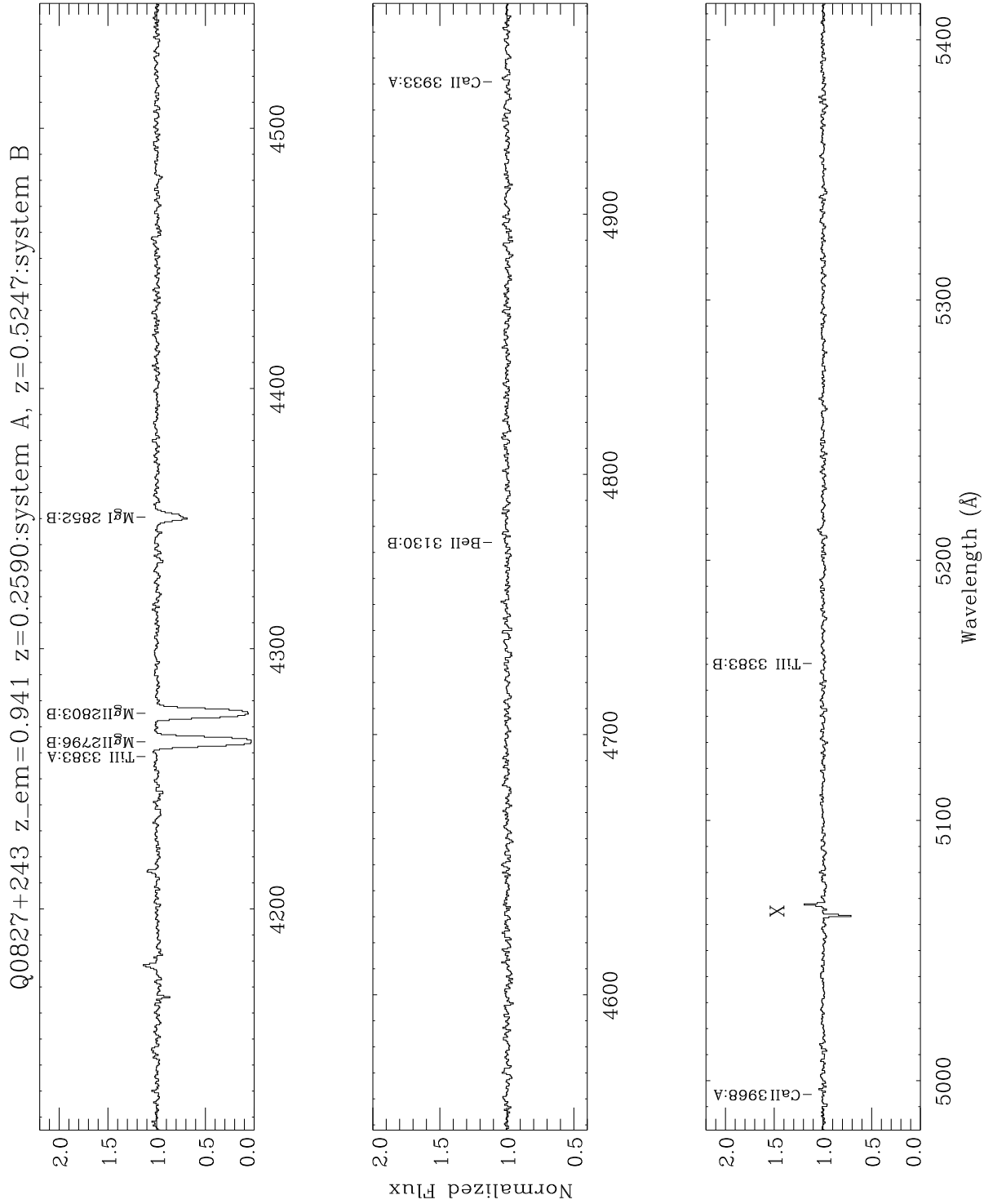


Figure 2. Same as Figure 1, but for Q0827+243.

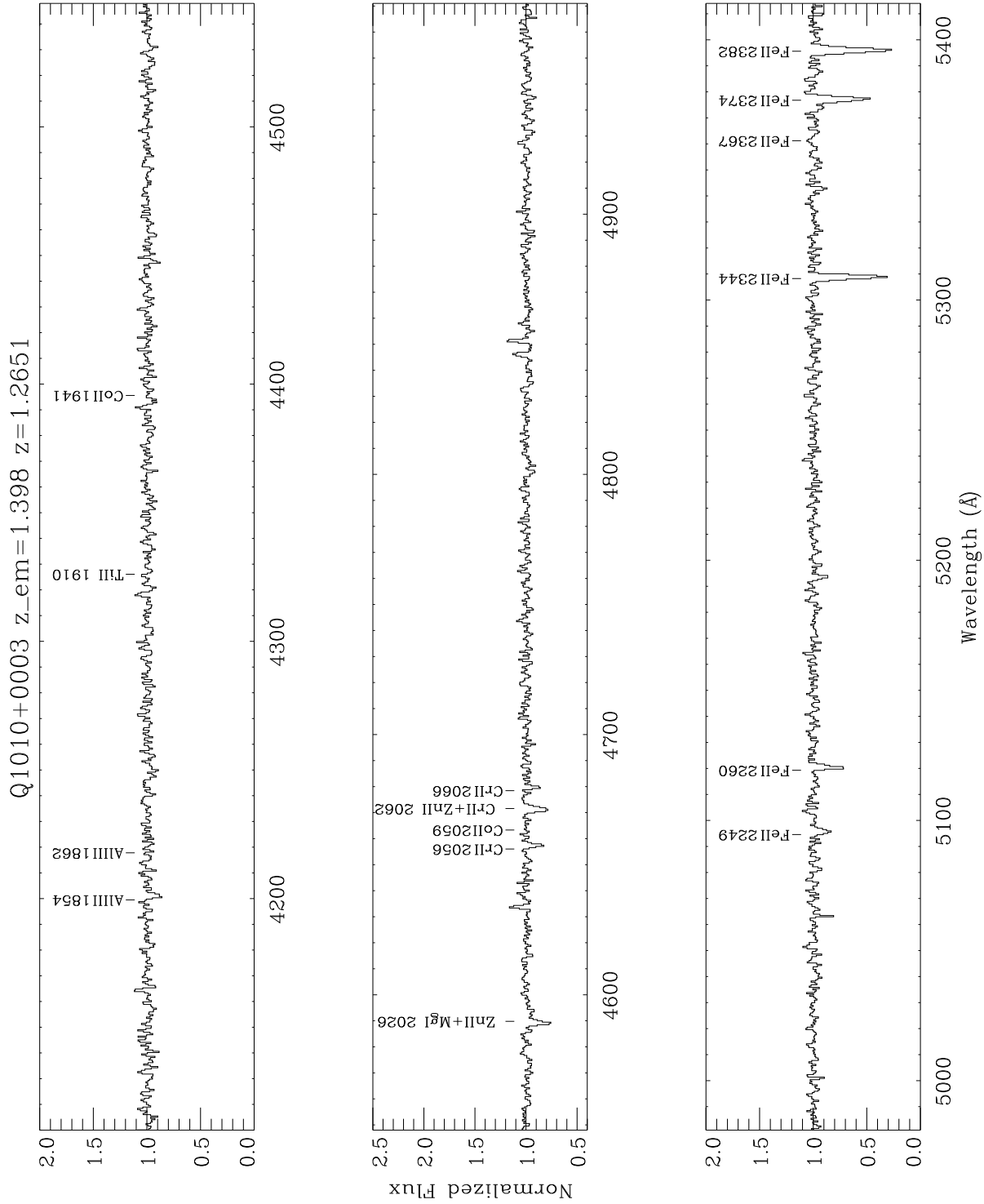


Figure 3. Same as Figure 1, but for Q1010+0003.

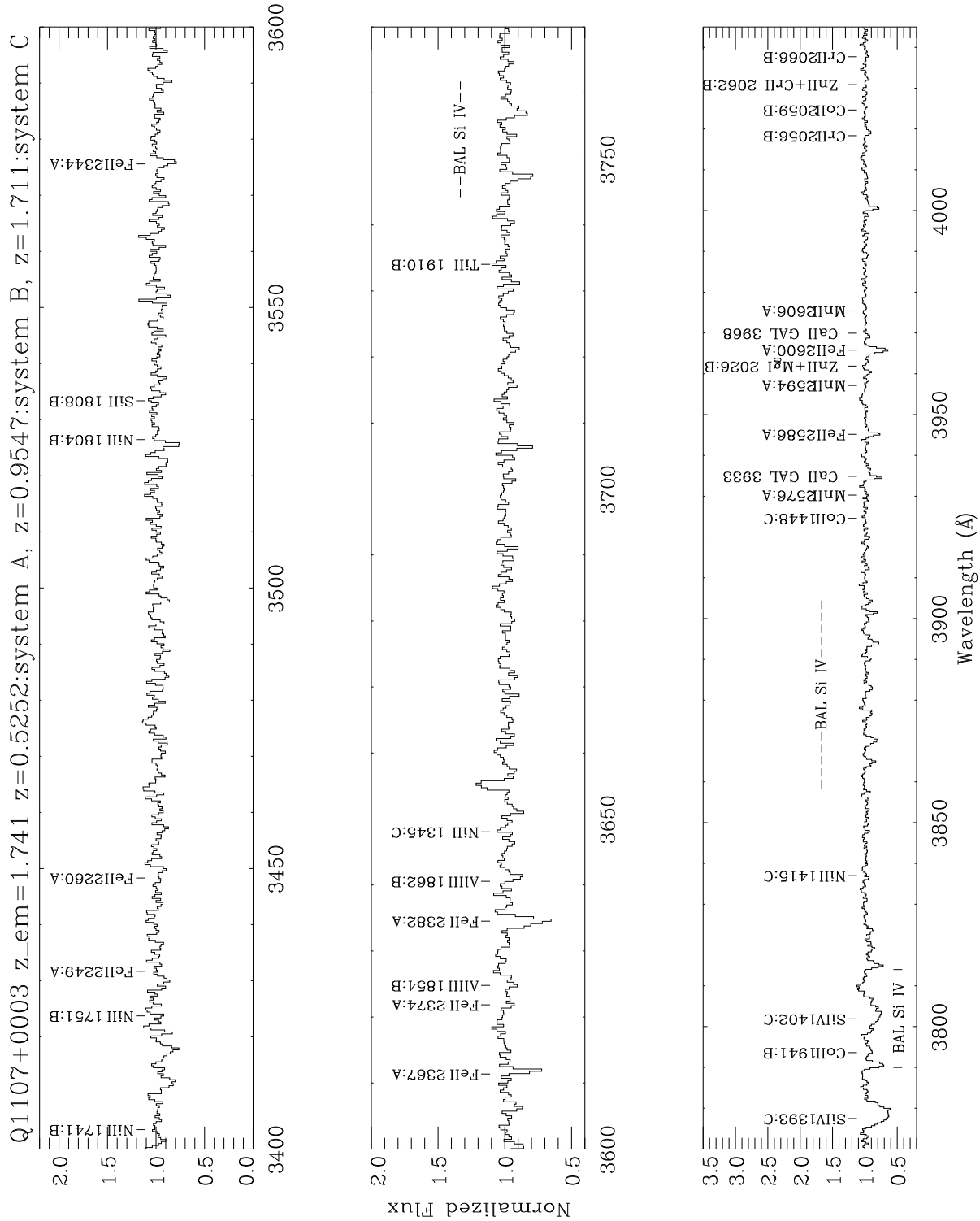


Figure 4. Same as Figure 1, but for Q1107+0003.

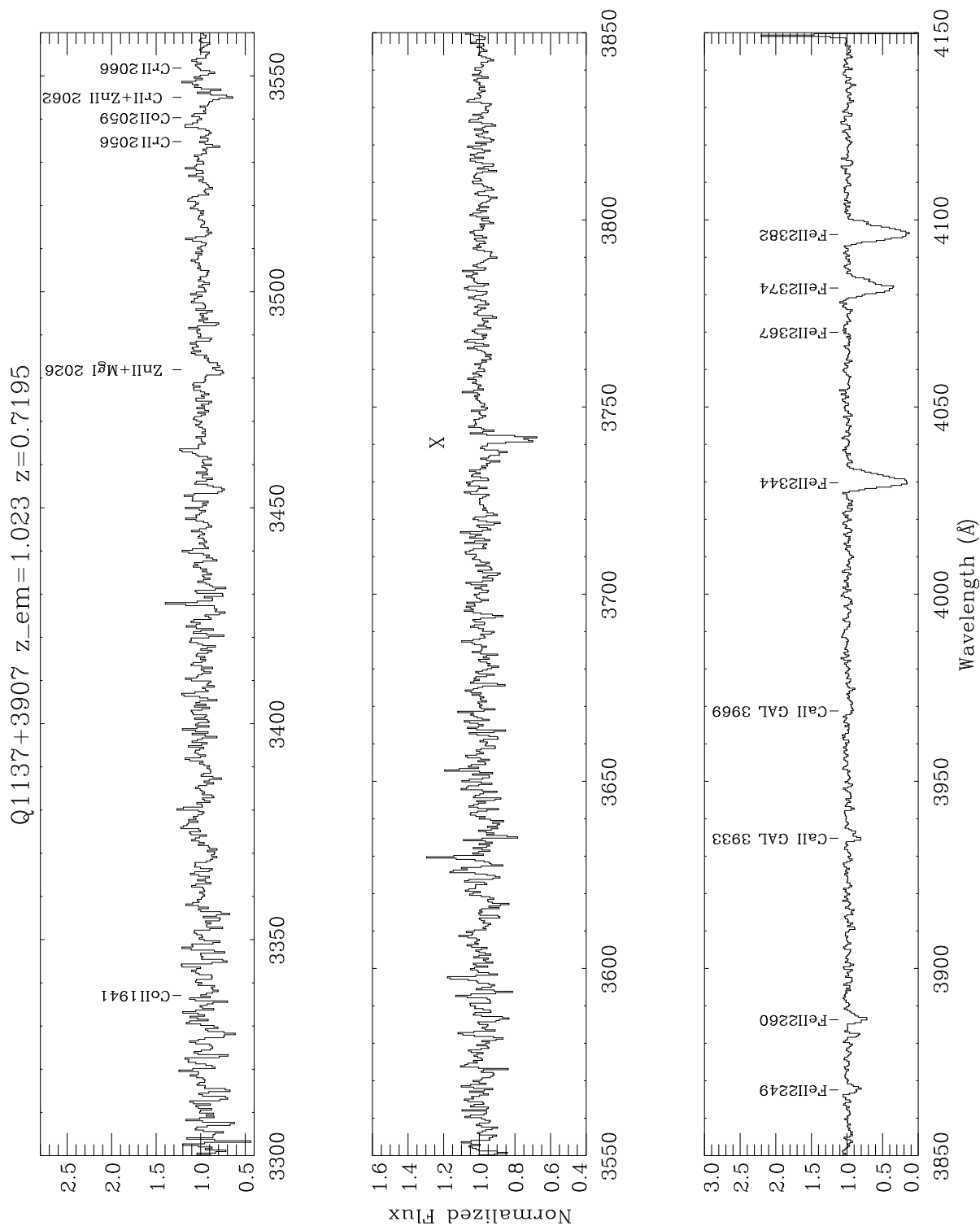


Figure 5. Same as Figure 1, but for Q1137+3907.

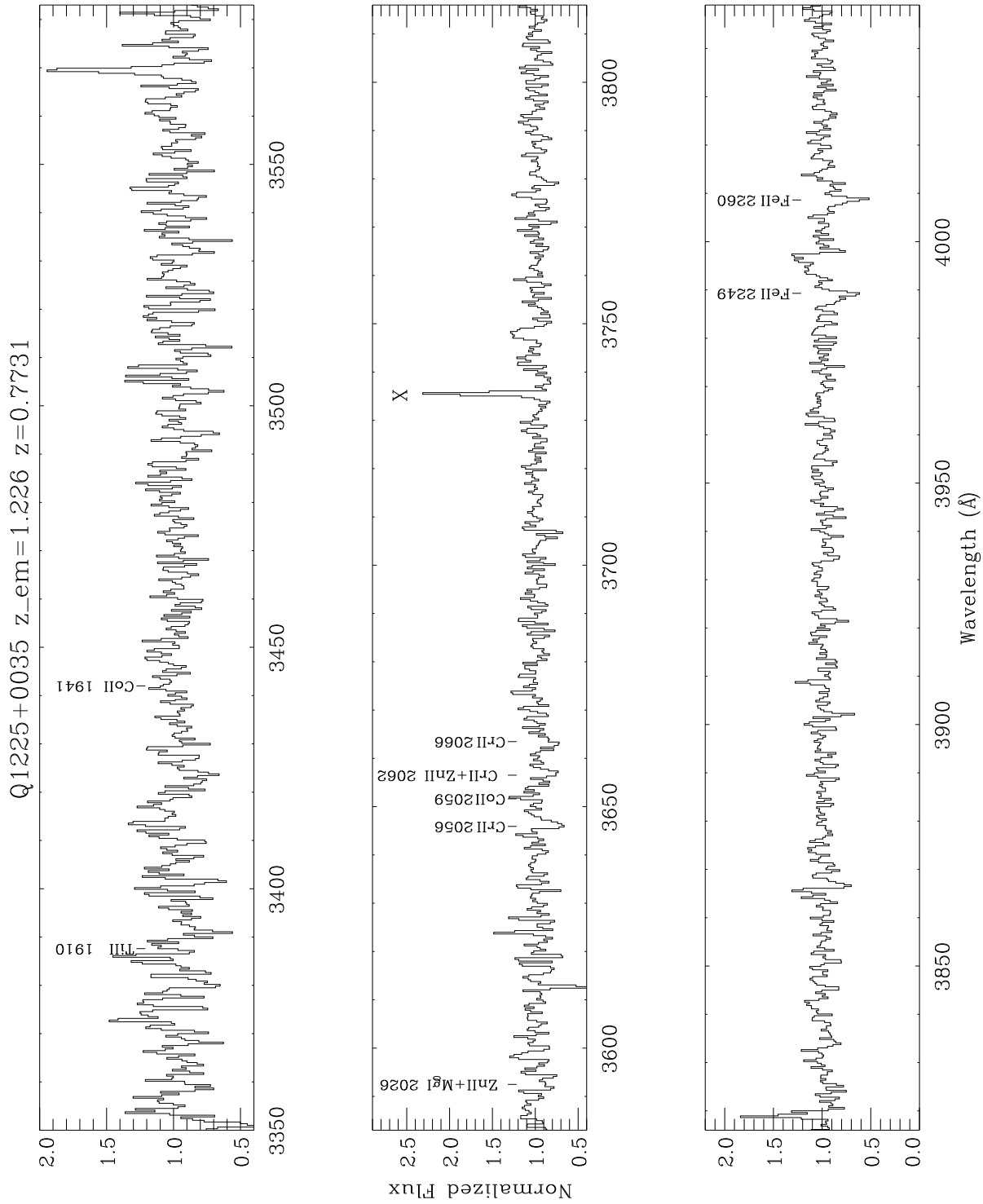


Figure 6. Same as Figure 1, but for Q1225+0035.

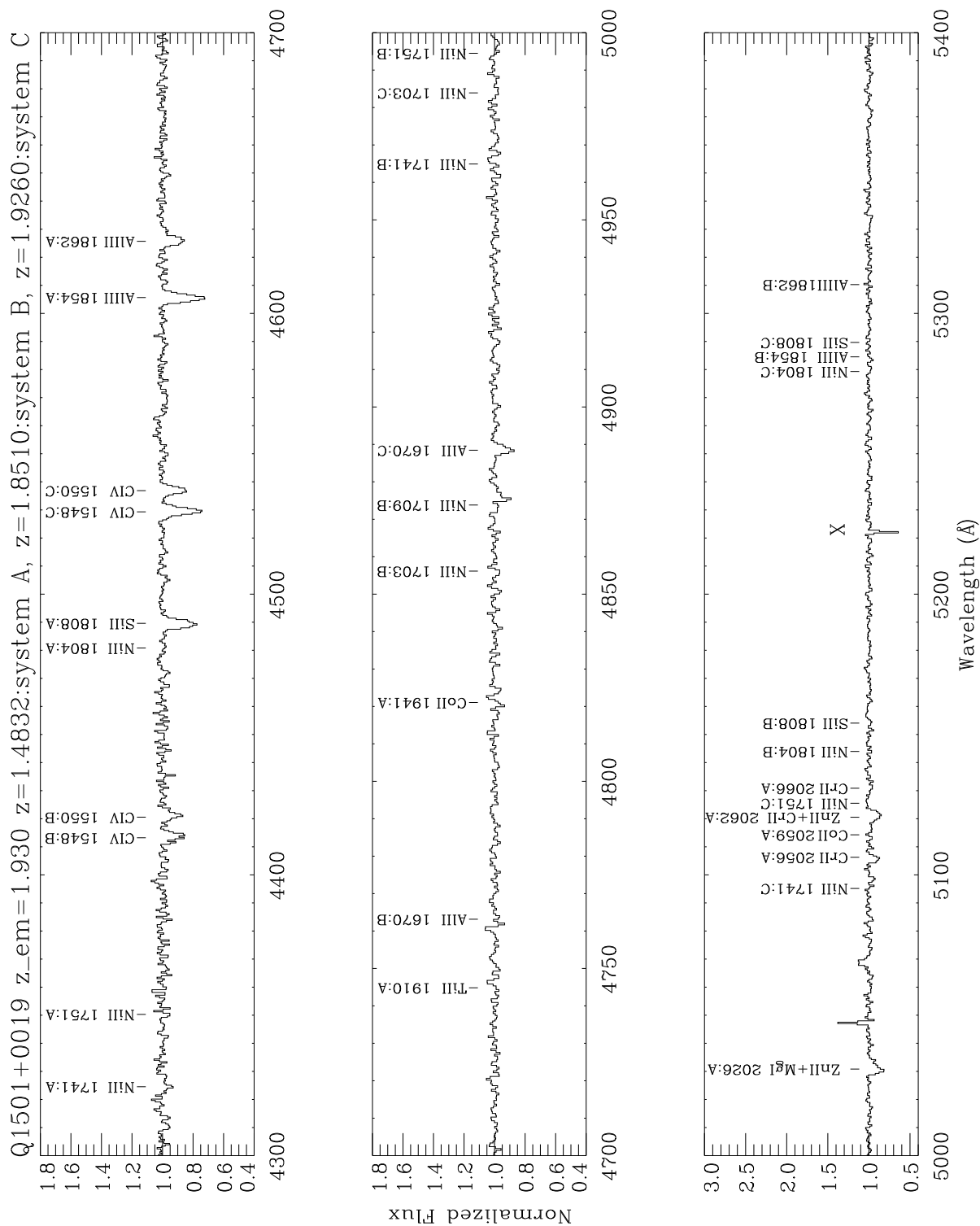


Figure 7. Same as Figure 1, but for Q1501+0019.

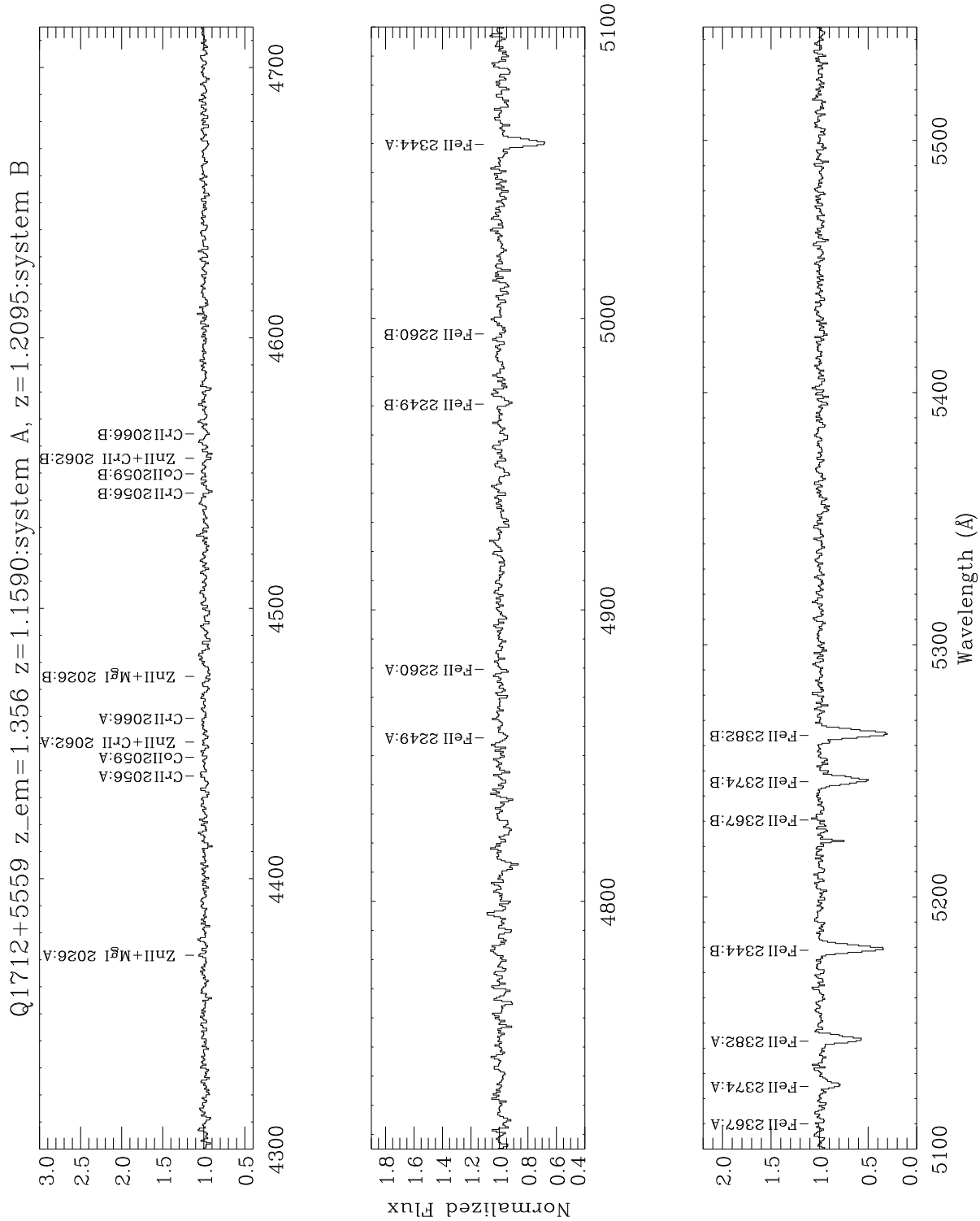


Figure 8. Same as Figure 1, but for Q1712+5559.

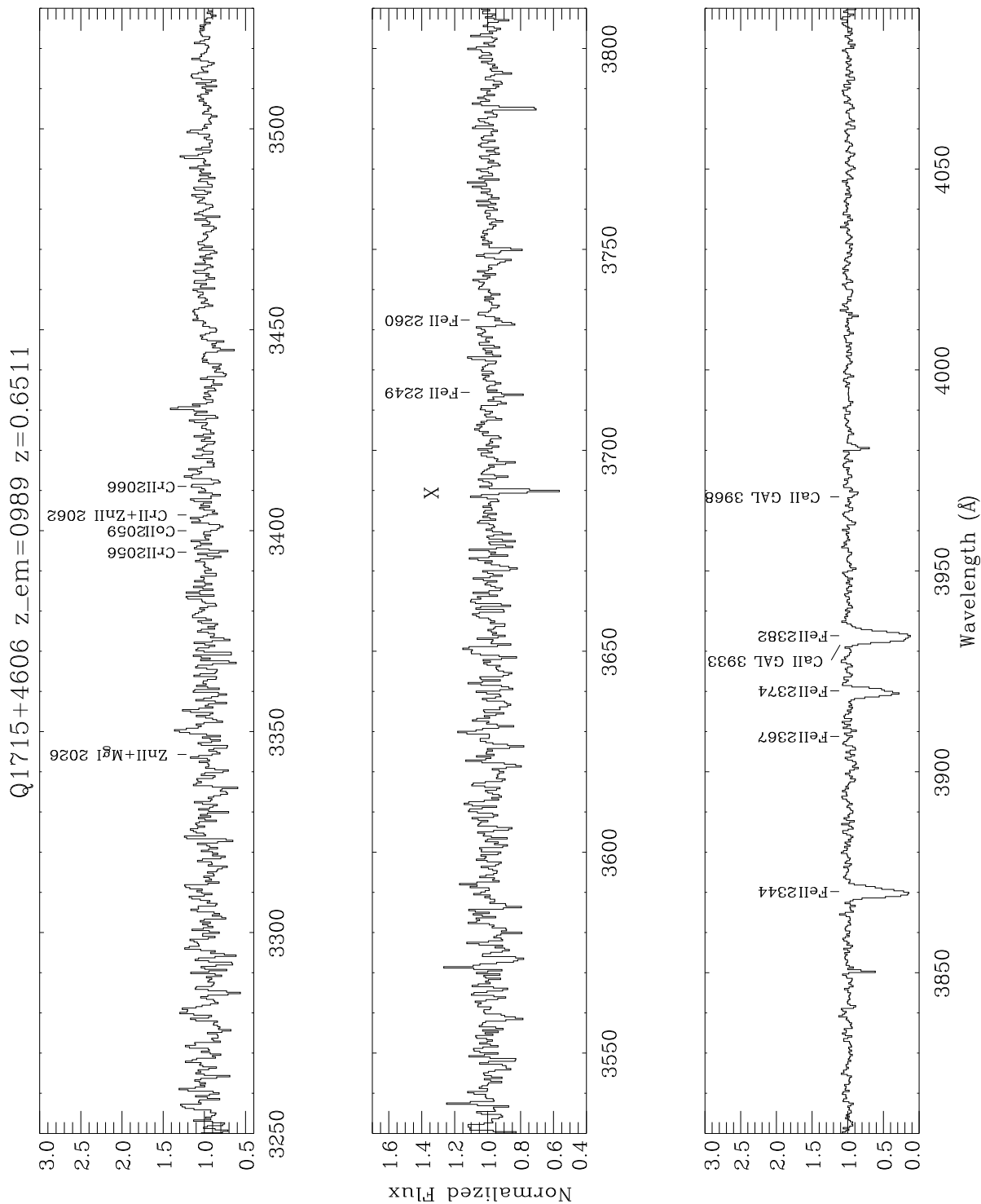


Figure 9. Same as Figure 1, but for Q1715+4606.

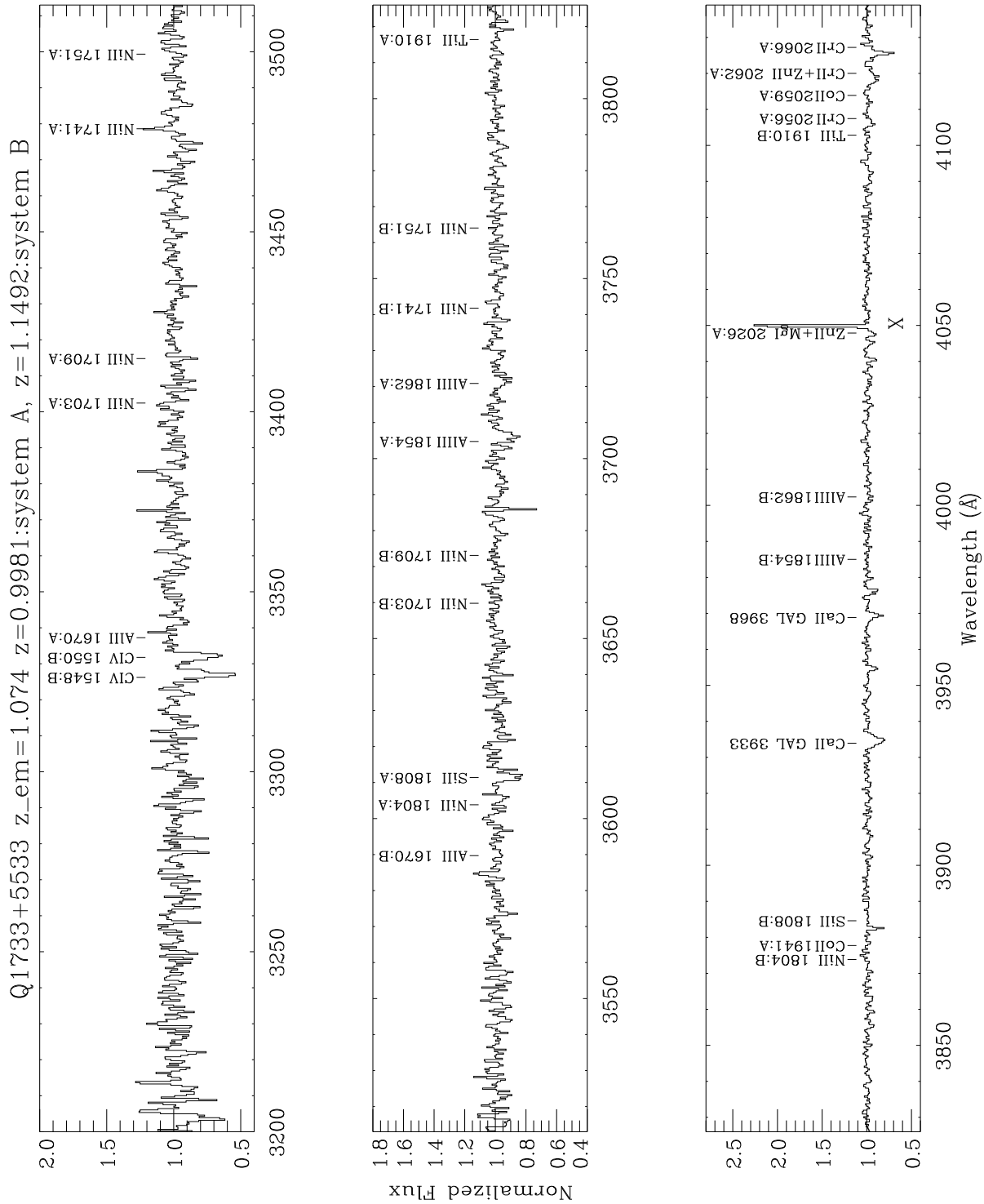


Figure 10. Same as Figure 1, but for Q1733+5533.

To judge the effect of potential saturation of Mg I λ 2852 we estimated the maximum N_{MgI} and hence the minimum N_{ZnII} as described in § 3. This gave log $N_{\text{ZnII}} > 12.95$, affirming the assumption that the Mg I contribution to the blended λ 2026 line is small. Fe II $\lambda\lambda$ 2249, 2260, 2344, 2374, 2382 lines were also detected.

Q1107 + 0003 ($z_{em} = 1.7408$, $z_{abs} = 0.5252$ for system A, $z_{abs} = 0.9547$ for system B and $z_{abs} = 1.711$ for system C): System B is of primary interest to this paper, and contains a confirmed sub-DLA from HST spectra with log $N_{\text{HI}} = 20.26$. This QSO also has a broad absorption line system (BAL) at $z \approx 1.711$. Si IV $\lambda\lambda$ 1393, 1403 lines from the BAL were detected. No Zn II or Cr II lines were detected from the sub-DLA at $z = 0.9547$, but upper limits were placed on the column densities. There is also a system at $z = 0.5252$ with weak Fe II lines detected in SDSS spectra. Lines of Fe II $\lambda\lambda$ 2344, 2382, 2586, 2600 were detected from this system. The weaker Fe II λ 2374 line however was not detected. The Fe II λ 2344, 2382 lines were fit simultaneously, as were the $\lambda\lambda$ 2586, 2600 lines with the same b_{eff} and v . Mn II $\lambda\lambda$ 2576, 2594, 2606 fell within the observable region for system B, but none were detected.

Q1137+3907 ($z_{em} = 1.023$ and $z_{abs} = 0.7193$): This is a BAL system. The Zn II + Mg I λ 2026 blend was detected at $\sim 3\sigma$ level in this system. The S/N in the region was ~ 15 , leading to larger errors in the column density estimates. There are no data available on Mg I for this system, so it could not be included in the fit of the blended Zn II+Mg I λ 2026. We are however confident of the Zn II column density quoted, because based on our experience so far, the contribution from Mg I λ 2026 is relatively small for most systems. For example, the $z = 1.2651$ DLA toward Q1010+0003 showed differences in the Zn II column density of only ~ 0.05 dex with and without the contribution from Mg I λ 2026. The Zn II λ 2026 line was fit using the b_{eff} value from the fit of the Fe II $\lambda\lambda$ 2249, 2260 lines. The Zn II component was held fixed in the blended λ 2026 line to determine N_{CrII} . Strong Fe II $\lambda\lambda$ 2249, 2260, 2344, 2374, 2382 were also detected. The feature at $\sim 3740 \text{ \AA}$ is caused by a defect in the CCD.

Q1225 + 0035 ($z_{em} = 1.226$ and $z_{abs} = 0.7730$): The spectra of this object were taken near daybreak, which resulted in additional noise due to increased background. The Cr II $\lambda\lambda$ 2056, 2062 lines was detected at $\sim 3\sigma$, allowing for moderately accurate determination of the column density. The Zn II+Mg I λ 2026 blend lies in a noisy region and was not detected, and the Zn II upper limit had to be estimated from S/N. We also detected Fe II λ 2249, 2260 lines which were fit simultaneously with the same b_{eff} and v . The feature at $\sim 3735 \text{ \AA}$ is caused by a defect in the CCD.

Q1501+0019 ($z_{em} = 1.930$, $z_{abs} = 1.4832$ for system A, $z_{abs} = 1.8510$ for system B, and $z_{abs} = 1.9260$ for system C): System A is the system of primary interest in this paper, and has a confirmed DLA from HST spectra. We detected only the C IV $\lambda\lambda$ 1548, 1550 lines in system B. The Zn II+Mg I λ 2026 blend, along with the Cr II+Zn II λ 2062 and Cr II λ 2056 lines were all detected in system A. Because the Cr II λ 2066 line was not detected, the Cr II column density was determined from Cr II λ 2056 solely. The Mg I contribution to the blended Zn II+Mg I λ 2026 line was determined from SDSS spectra, which yields a W_{rest} for the Mg I λ 2852 line of 952 m\AA . This line was fit using a one component model, giving log $N_{\text{MgI}} = 12.93 \pm 0.05$. This component was held fixed in the MMT spectrum of the λ 2026 line while the Zn II and Cr II $\lambda\lambda$ 2056, 2062, and 2066 lines were fit simultaneously. To judge the effects of saturation of Mg I λ 2852, we again estimated the maximum Mg

I contribution to the blended λ 2026 line as described in § 3. This gave $N_{\text{ZnII}} > 12.89$, only 0.04 dex less than the “best fit” model. Al III $\lambda\lambda$ 1854, 1862 lines were also detected and fit together while simultaneously varying N , b_{eff} , and v . The feature at $\sim 5220 \text{ \AA}$ is caused by a defect in the CCD.

Q1712 + 5559 ($z_{em} = 1.930$, $z_{abs} = 1.2093$ for system A and $z_{abs} = 1.1584$ system B): System A is the system of primary interest for this paper, and contains a confirmed DLA from HST spectra with log $N_{\text{HI}} = 20.72$. Both systems contain strong Fe II $\lambda\lambda$ 2344, 2374, 2382 lines. No other lines from system B appear to be present. No Zn II or Cr II lines were detected in either system, with S/N ~ 30 in the region. The feature at $\sim 5220 \text{ \AA}$ is caused by a defect in the CCD.

Q1715 + 4606 ($z_{em} = 0.989$ and $z_{abs} = 0.6511$) We have determined the H I column density for this object from archival HST data. By fitting the line profile, we have determined a column density of log $N_{\text{HI}}=20.44$. Strong Fe II $\lambda\lambda$ 2344, 2374, 2382 lines were detected. No lines of Zn II or Cr II were seen, although the S/N in the region was only ~ 10 due to poor weather during the observations. A weak Galactic Ca II λ 3698 feature was seen, but the stronger Ca II λ 3933 line was blended with the Fe II λ 2382 line from the $z_{abs}=0.6511$ system. The feature located at $\sim 3690 \text{ \AA}$ is an artifact of the CCD.

Q1733 + 5533 ($z_{em} = 1.074$ and $z_{abs} = 0.9984$ for system A and $z_{abs} = 1.1496$ for system B) System A is of primary interest for this study, as it has a confirmed DLA with log $N_{\text{HI}} = 20.70$. System B appears to be a C IV system with no other absorption features at this redshift detected in SDSS spectra. No Zn II or Cr II lines were detected in system A, but the relatively high S/N (~ 33) in the region allows us to place tight upper limits on the abundances. Al III $\lambda\lambda$ 1854,1862 lines were weakly detected and were fit together varying N , b_{eff} , and v simultaneously. We also detected strong Galactic Ca II λ 3933, 3968 lines.

5 RESULTS AND DISCUSSION

5.1 Relative Abundances

The observed relative abundances of the elements are a combination of both the nucleosynthetic processes and of dust depletion. If dust is significantly present in DLAs, then refractory elements such as Cr, Mn, Fe, Co, and Ni should show substantial depletions. As already discussed in § 1, Zn is a relatively undepleted element due to its low condensation temperature. Ratios such as [Cr/Zn] and [Fe/Zn] are therefore a measure of dust depletion. Table 5 lists abundances of Cr, Fe, and Ti relative to Zn for the systems in our sample. Also given is the metallicity [Zn/H]. Although it is customary to estimate metallicity based on measurements of N_{ZnII} , it has been shown that [Zn/H] is not much affected by ionization (Vladilo et al. 2001).

No Ti II was found in any of the systems sampled. We determined [Ti/Zn] upper limits of -1.01 and -1.24 for the DLAs toward Q1010+0003 and Q1501+0019 respectively. The measured [Fe/Zn] in Q1010+0003 was also sub-solar (-0.69) also suggesting dust depletion. No Fe lines were sampled in the spectra of Q1501+0019, so [Fe/Zn] could not be measured.

Si is an α -capture element, and its abundance relative to Fe group elements can provide clues into the chemical evolution of DLAs. Disk stars in the Milky Way show a systematic decrease in $[\alpha/\text{Fe}]$ with increasing [Fe/H], which indicates an increase with time of Fe contributed to the ISM from type Ia supernovae, relative to type II supernovae (Edvardsson et al. 1993). Prochaska

Table 4. Column Densities

QSO	z_{abs}	Species	$\log N$ cm^{-2}	b_{eff} km s^{-1}	QSO	z_{abs}	Species	$\log N$ cm^{-2}	b_{eff} km s^{-1}	
0738+313	0.0912	Ca II	12.32±0.02	51.2	1225+0035	0.7731	Mg I	12.85±0.06 ^c	52.4	
		Ti II	12.53±0.10 ^a	...			Cr II	13.99±0.11	74.7	
		Cr II	13.28±0.22 ^b	...			Fe II	15.69±0.03	74.7	
		Zn II	<12.66 ^a	...			Zn II	<13.01	...	
	0.2210	Mg I	12.00±0.10 ^a	...		1501+0019	1.4832	Mg I	12.92±0.05 ^c	96.6
		Mg II	>13.30±0.03 ^a	...				Al III	13.35±0.01	87.1
		Ca II	11.91±0.03	34.2				Si II	15.71±0.02	86.5
		Ti II	<11.48	...				Cr II	13.40±0.09	86.5
		Cr II	13.11±0.24 ^b	...				Zn II	12.93±0.06	86.5
		Zn II	<12.83 ^b	...				1.8510	C IV	13.64±0.04
0827+243	0.2590	Ca II	<11.60	...	1.9260	C IV	13.87±0.03	88.8		
		Ti II	<11.96	...		Al II	12.33±0.04	53.4		
	0.5247	Mg I	12.69±0.02	80.3	1712+5559	1.1584	Cr II	<12.93	...	
		Mg II	>14.59	80.3			Fe II	13.98±0.03	74.9	
Ti II		<11.76	...	Zn II			<12.25	...		
Cr II		<13.42 ^b	...	1.2093			Mg I	12.44 ^c	76.7	
1010+0003	1.2651	Fe II	14.59±0.02 ^a	...	1715+4606	GAL ^d	Cr II	<12.86	...	
		Zn II	<12.80 ^b	...			Fe II	>14.54	76.7	
		Mg I	12.67±0.05 ^c	184.3			Zn II	<12.19	...	
		Al III	12.67±0.10	10.8			Ca II	12.66±0.10	35.5	
		Cr II	13.54±0.07	22.5			0.6511	Cr II	<13.54	...
		Fe II	15.26±0.05	22.5			Fe II	14.94±0.03	57.4	
1107+0003	0.5252	Zn II	12.96±0.06	22.5	1733+5533	GAL ^d	Zn II	<12.87	...	
		Mn II	<12.16	...			Ca II	12.79±0.03	88.2	
	0.9547	Fe II	13.54±0.08	37			0.9984	Mg I	12.44 ^b	...
		Ti II	<13.01	...				Al III	13.13±0.05	133.7
		Cr II	<12.76	...				Si II	15.48±0.06	118.9
		Zn II	<12.08	...				Cr II	<12.79	...
1137+3907	1.7110	Si IV	13.99±0.03	198.3	1.1496	Zn II	<12.11	...		
	GAL ^d	Ca II	12.63±0.05	87.8		C IV	14.19±0.04	88.8		
	0.7193	Cr II	13.71±0.20	122.9		Al II	<11.77	...		
		Fe II	15.45±0.05	122.9		Si II	<14.6	...		
		Zn II	13.43±0.05	122.9	

^a: Khare et al. (2004) ^b: Kulkarni et al. (2005) ^c: From SDSS spectra. ^d: Entries with GAL identifier are from lines originating in the Milky Way.

& Wolfe (1999) observed that the DLAs in their sample showed no such trend, and that most of the objects were α -enhanced. In DLAs, Zn is a better indicator of Fe group abundances than Fe because of the large depletion of Fe on dust grains. We detected Si II λ 1808 in Q1501+0019 and Q1733+5533. [Si/H] = -0.68 in Q1501+0019, and [Si/H] = -0.76 in Q1733+5533. We unfortunately did not cover any Fe II lines in the region. However, [Si/Zn] = -0.28 in Q1501+0019, and [Si/Zn] > 0.37 in Q1733+5533, implying significant α -enhancement in the latter system.

Figure 11 shows [Cr/Zn] vs. [Zn/H] for our data as well as those from the literature. Only detections, not limits have been plotted. There is intrinsic scatter in the data, which is to be expected, but there appears to be a general trend suggesting that the most metal rich DLAs also show the most depletion. If this is true, then one would expect the most metal rich absorbers to be under-sampled because they would also most likely be the most reddened. A Spearman rank-order correlation test on the 48 data points plotted in Fig. 11 gives the Spearman rank-order coefficient $R_S = -0.623$, with a probability of obtaining such a value by chance of $P(R_S) = 1.95 \times 10^{-5}$.

Figure 12 shows [Fe/Zn] vs [Zn/H] for our data as well as from the literature. Again, only detections have been plotted. Both

figures 11 and 12 show a trend toward higher depletion with higher metallicity. Previous investigations have shown a similar anti-correlation between [Cr/Zn] or [Fe/Zn] and [Zn/H] although the vast majority of their data set has come from absorbers at $z > 1.5$ (Pettini et al. 1997; Prochaska & Wolfe 2002; Akerman et al. 2005). Our study increases the number of Zn measurements at $z < 1.0$ by $\sim 30\%$. A Spearman rank-order correlation test on this data set gives $R_S = -0.428$, with a probability of obtaining such a value by chance of $P(R_S) = 6.00 \times 10^{-3}$.

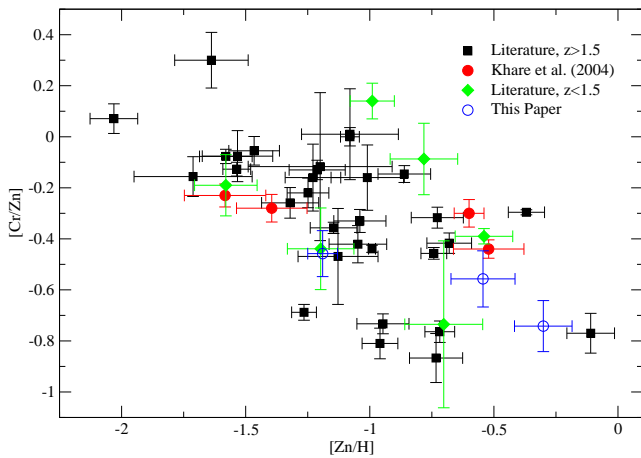
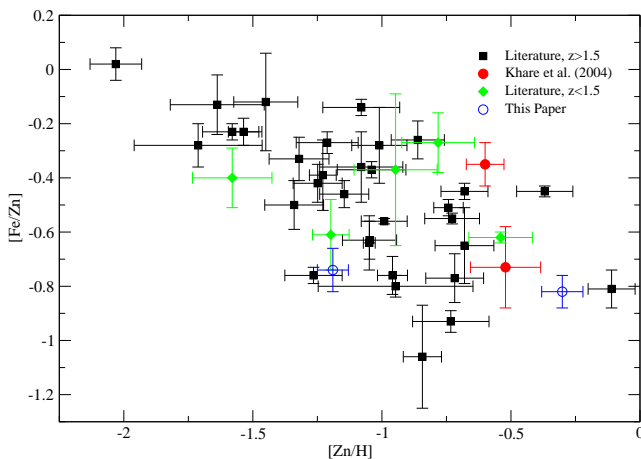
5.2 Dust Obscuration Bias

Several studies have tried to understand whether current DLA observations are affected by a dust obscuration bias. Recently, York et al. (2006) conducted a survey of 809 Mg II systems from the SDSS with $1.0 \leq z \leq 1.9$ and found that QSOs with an intervening absorber are at least three times more likely to have highly reddened spectra than QSOs without any absorption systems in their spectra. Furthermore, York et al. (2006) found a trend toward higher Zn II column densities but lower [Zn/H] and lower abundances of the first ions as the reddening E(B-V) increased. Significant red-

Table 5. Relative Abundances

QSO	z_{abs}	[Zn/H]	[Cr/Zn]	[Fe/Zn]	[Ti/Zn]	[Si/Zn]
Q0738+313	0.0912	<-1.14 ^a	>-0.21 ^a	>-0.48 ^a
...	0.2213	<-0.7 ^a	<0.7 ^a
Q0827+243	0.5247	<-0.04 ^a	<-0.3 ^a
Q1010+0003	1.2651	-1.19	-0.46	-0.54	<-1.01	...
Q1107+0003	0.9547	<-0.72
Q1137+3907	0.7190	-0.30	-0.67	-0.82
Q1225+0035	0.7731	<-1.15	>0.09	>0.07
Q1501+0019	1.4832	-0.54	-0.56	...	<-1.24	-0.28
Q1712+5559	1.2093	<-1.07	...	>-0.51
Q1715+4606	0.6511	<-0.61	...	>-0.78
Q1733+5533	0.9981	<-1.13	>0.37

^a: Abundance measurements from Kulkarni et al. (2005).


Figure 11. [Cr/Zn] vs. [Zn/H] for our data as well as measurements from the literature. Only detections are plotted.

Figure 12. [Fe/Zn] vs. [Zn/H] for our data as well as from the literature. Only detections are plotted.

dening has also been seen in a sample of strong Ca II absorbers (Wild & Hewett 2005; Wild et al. 2006).

If dust obscuration effects are significant, highly reddened QSOs would be under-sampled due to their faintness. Boisse et al. (1998) pointed out that there is a deficit of systems with high N_{HI} and high [Zn/H], and suggested that this may be caused by a dust obscuration bias (because such systems may also have high dust content and may obscure the background quasars more). They speculated that observations of fainter QSOs might reveal systems with high N_{HI} and high metallicity. Figure 13 shows a plot of [Zn/H] vs. N_{HI} for DLAs from our sample as well as the literature (Akerman et al. 2005, Rao et al. 2005). Clearly, there is a deficit of systems that are seen with both low metallicity and low N_{HI} . This could be attributed to observational limitations in detecting weak Zn II lines, although recent high resolution, high S/N observations still find a dearth of systems in this region. More interestingly though, there are few absorbers with high metallicity and high N_{HI} , as noted by Boisse et al. (1998) and also by Akerman et al. (2005). This cannot be credited to observational limitations, because systems with similar metallicities have been detected at lower N_{HI} , and seems to suggest that these types of systems are being under-sampled. Also, there is nothing unphysical about systems with high N_{HI} and high metallicity. It is thus surprising that only 3 points from the literature (of which 1 came from our previous sample in Khare et al. 2004) lie above the dashed line indicating the empirical ‘‘obscuration threshold’’ $\log N_{\text{ZnII}} < 13.15$ suggested by Boisse et al. (1998).

Two of the systems at $z < 1.5$ that lie above the ‘‘obscuration threshold’’ came from our samples (this paper and Khare et al. 2004), although it is still remarkable that all points in Fig. 13 lie fairly close to the threshold suggested by Boisse et al. (1998). Indeed, all but two of the points are consistent, within the errors, with being below the obscuration threshold. It should also be noted that the Boisse et al. threshold is not meant to be a hard limit, but an observationally determined boundary based on the much smaller sample available to Boisse et al. (1998). Indeed, hydrodynamical simulations by Cen et al. (2003) predict the existence of absorbers above this threshold. Thus, it may not be completely surprising that we are now finding some objects above the threshold.

We emphasize that the higher proportion of systems with N_{ZnII} close to the Boisse et al. threshold in our studies (this paper and Khare et al. 2004) is not due to errors in the column density estimations from the moderate resolution of the MMT spectrograph. Column densities derived from our observations of several systems with both the MMT and with the higher resolution ($\sim 5 \text{ km s}^{-1}$)

Ultraviolet-Visual Echelle Spectrograph (UVES) on the Very Large Telescope (VLT) agree to within 0.1 dex (Poux et al. 2006a,b). A similar agreement was also found between column densities derived by Khare et al. (2004) from MMT spectra and those derived by Rao et al. (2005b) from Keck HIRES spectra. The reason for the higher proportion of metal-rich systems in our studies is that the targets in this paper and Khare et al. (2004) were chosen partially because of strong metal line absorption features seen in SDSS spectra. Thus, these systems may have been more likely to have higher Zn column densities. Indeed, composite SDSS quasar spectra indicate that systems with larger W_{rest} of Mg II $\lambda 2796$ tend to have stronger Zn II lines (Nestor et al. 2003; York et al. 2006). One of our two systems has a large depletion consistent with the obscuration selection effect while the other system shows a moderate depletion, so it is not clear whether the small number of such systems found so far is caused by dust obscuration or small sample size especially at $z < 1.5$ where the effects of dust are expected to be the most pronounced (Boisse et al. 1998). It could also be the case that the most metal rich systems are truly rare.

Figures 14 and 15 show the dust content as measured by [Cr/Zn] and [Fe/Zn] respectively vs. $\log N_{\text{HI}}$ for these DLAs as well as those from the literature. As can be seen, there is very little trend in the data. It may appear surprising from Figs. 11-15 that there is no (anti)-correlation between [Cr/Zn] (or [Fe/Zn]) and $\log N(\text{HI})$ even though there is an (anti)-correlation between [Cr/Zn] (or [Fe/Zn]) and [Zn/H] and between [Zn/H] and $\log N_{\text{HI}}$. If one traces some of the extreme points in Figs. 11 (or 12) and 13 that do show the correlation, one can see that the correlations in these two figures arise from different systems. For example, consider the 3 points A, B, and C with ([Cr/Zn], [Zn/H], $\log N_{\text{HI}} \approx (-0.46, -1.19, 21.52)$; $(-0.74, -0.30, 21.10)$; and $(-0.54, -.57, 20.85)$. Points such as A and B are responsible for the correlation in Fig. 11. Points such as B and C are responsible for the correlation in Fig. 13. When one plots these points in Fig. 14, there is no strong correlation. (More generally, if data sets x,y and y,z show correlations, x and z do not necessarily show a correlation; whether or not they do depends on the distribution of the individual data values. See, for example, Casella & Berger 2002.)

5.3 Constraints on Metallicities and Potential Implications for Metallicity Evolution

The Zn abundances for our DLAs are listed in Table 5. In 4 of the systems at $0.6 < z < 1.5$ the abundances of Zn are about 10% solar or lower, while in 2 systems, the abundances are 30-50 % solar. We now briefly discuss the implications of our data for the metallicity evolution of DLAs. Our analysis is based on the statistical procedures outlined in Kulkarni & Fall (2002), and uses our data, the data compiled in Kulkarni et al. (2005), and other recent data from the literature (Rao et al. 2005; Akerman et al. 2005). We binned the combined sample of 109 DLAs in 6 redshift bins with 18 or 19 systems each and calculated the global N_{HI} -weighted metallicity in each bin. Figure 16 shows [Zn/H] vs. z for the data in the literature as well as from this paper.

We constructed two samples for these 109 DLAs: a “maximum limits” sample where the Zn limits are treated as detections, and a “minimum limits” sample, where the Zn limits are treated as zeros. For an individual system these extreme cases cover the full range of possible values the Zn column densities can take in the case of the limits. The N_{HI} -weighted mean metallicity in the lowest redshift bin $0.1 < z < 1.2$ is -0.78 ± 0.11 for the “maximum limits” sample and -0.99 ± 0.17 for the “minimum limits”

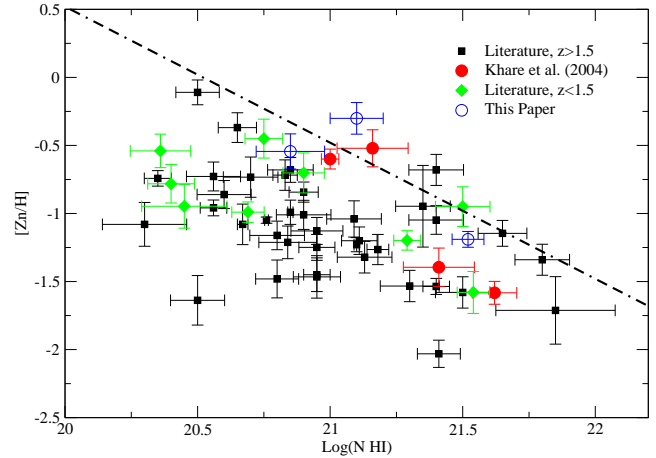


Figure 13. [Zn/H] vs. $\log N_{\text{HI}}$ for our data as well as previous measurements from the literature. The dashed line indicates the empirical upper limit $\log N_{\text{ZnII}} < 13.15$ inferred from previous studies and suspected to be the “obscuration threshold”. Only detections are plotted.

sample. The linear regression slope of the metallicity-redshift relation for the redshift range $0.1 < z < 3.9$ is -0.18 ± 0.07 for the “maximum limits” sample, and -0.25 ± 0.10 for the “minimum limits” sample. The corresponding estimates for the intercept of the metallicity-redshift relation are -0.65 ± 0.15 for the “maximum limits” sample and -0.63 ± 0.21 for the “minimum limits” sample. Thus our data support the conclusions of Khare et al. (2004) and Kulkarni et al. (2005) that the global mean metallicity of DLAs shows at best a slow evolution with redshift.

6 CONCLUSIONS AND FUTURE WORK

The MMT observations presented here, together with our previous MMT and HST data have more than doubled the DLA Zn sample at $z < 1.5$ and more than tripled the sample at $z < 1$. Combining our data with data from the literature, we find that the systems with higher [Zn/H] also have stronger Cr depletion [Cr/Zn]. Analysis of the N_{HI} -weighted mean metallicity vs. redshift for our sample combined with previous data from the literature supports previous conclusions that the N_{HI} -weighted mean global DLA metallicity rises slowly at best and does not reach solar levels by $z = 0$.

Questions still remain pertaining to dust depletion and selection effects, and linked to this, the metallicity-redshift relationship of DLAs. Despite the large improvement from our surveys, DLA samples at $z < 1.5$ are still relatively small. Clearly, more observations of DLAs at $z < 1.5$ are needed for improved statistics in this vast epoch (~ 9 Gyr). The large number of SDSS absorbers now available present a good opportunity for this purpose.

Two of our systems have higher N_{ZnII} than the empirical upper limit ($\log N_{\text{ZnII}} < 13.15$) that has been attributed to dust obscuration in previous studies. The fairly high Zn abundances in these 2 DLAs suggests that metal-rich DLAs may be a rare class of objects, but can be found in a large enough sample. It would be interesting to confirm the metal-rich nature of these DLAs with higher resolution spectra in the future, and find similar other systems by observing a larger sample. If a large number of such systems are found, they may make a significant contribution to the cosmic budget of metals.

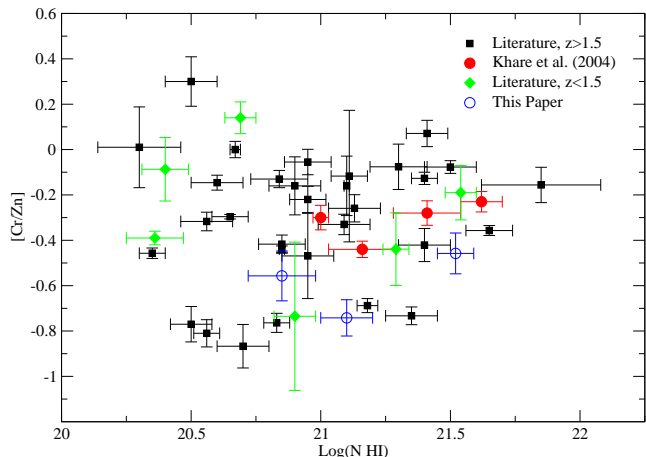


Figure 14. [Cr/Zn] vs. $\log N_{\text{HI}}$ for our data as well as measurements from the literature. Only detections are plotted.

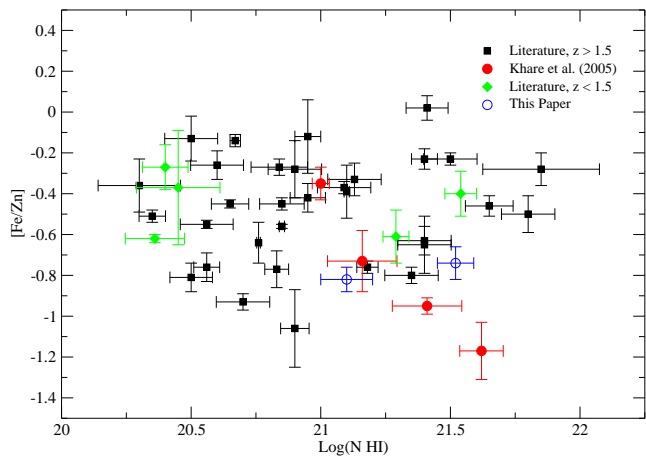


Figure 15. [Fe/Zn] vs. $\log N_{\text{HI}}$ for our data as well as measurements from the literature. Only detections are plotted.

It has been suggested that the low metallicity found in DLAs is caused by metallicity gradients. On the basis of a small sample of objects Chen et al. (2005) reported a difference between emission line and absorption line metallicities. If metallicity gradients are present in DLAs, then metal poor DLAs may be more likely to be found because larger impact parameters are more probable. This may be because (a) they correspond to larger cross-sections and (b) they correspond to less dust. On the other hand, other studies (Schulte-Ladbeck et al. 2005; Bowen et al. 2005) have found no difference between emission and absorption line metallicities for other DLAs. Given that the metallicity gradients are not well established and fairly weak even in nearby spirals, it is not clear if metallicity gradients fully explain the low metallicities seen in DLAs.

So far, no DLA has been observed with a super-solar metallicity. The key to finding such systems may lie in observing faint, reddened QSOs. Vladilo & Péroux (2005) have estimated that dusty

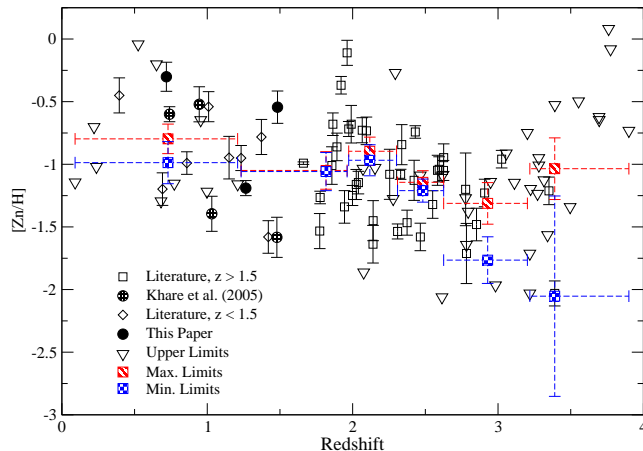


Figure 16. The metallicity [Zn/H] vs. z for the DLAs in this sample as well as from the literature.

DLAs may contribute as much as 17 % of the total metals. $\Delta(g - i)$ measurements are available from SDSS photometry for thousands of quasars with candidate DLAs and sub-DLAs. It would be interesting to obtain [Cr/Zn] and [Fe/Zn] for a large sample of such objects to study dust depletion patterns in quasar absorbers and to examine trends between quasar reddening and dust depletion.

ACKNOWLEDGMENTS

We thank the staff of the MMT observatory for assistance during our observing runs. We thank C. Péroux for helpful comments on an earlier version of this paper and J. Grego for discussions on statistical techniques. JM and VPK gratefully acknowledge support from the National Science Foundation grant AST-0206197 and the NASA/STScI grant GO-9441. PK acknowledges support from the University of South Carolina Research Foundation during a visit there in Spring and Summer 2004. We also would like to thank the anonymous referee for the insightful and helpful comments concerning this paper.

REFERENCES

Abazajian K., Adelman J., Agueros M., et al., 2005, *AJ*, 129, 1755
 Akerman C.J., Ellison S.L., Pettini M., Steidel C.C., 2005, *A&A*, 440, 449
 Bergeson S.D., Lawler J.E., 1993a, *ApJ*, 408, 382
 Bergeson S.D., Lawler J.E., 1993b, *ApJ*, 414, L137
 Bergeson S.D., Mullman K.L., Lawler J.E. 1994, *ApJ*, 435, L157
 Bergeson S.D., Mullman K.L., Wickliffe M.E., Lawler J.E., Litzen U., Johansson S. 1996, *ApJ*, 464, 1044
 Boisse P., Le Brun V., Bergeron J., Deharveng J., 1998, *A&A*, 333, 841
 Bowen D.V., Jenkins E.B., Pettini M., Tripp T.M., 2005, *ApJ*, 635, 880
 Casella G., Berger R.L., *Statistical Inference* 2nd ed., Duxbury, 2002
 Cen R., Ostriker J., Prochaska J.X., Wolfe A., 2003, *ApJ*, 741, 598

- Edvardsson B., Anderson J., Gustafsson B., Lambert D.L., Nissen P.E., Tompkin J., 1993, *A&A*, 275, 101
- Khare P., Kulkarni V.P., Lauroesch J.T., York D.G., Crotts P.S., Nakamura O., 2004, *ApJ*, 616, 86
- Kulkarni V.P., Fall S.M., Lauroesch J.T., York D.G., Welty D.E., Khare P., Truran J.W., 2005, *ApJ*, 618, 68
- Lodders K. 2003, *ApJ*, 591, 1220
- Mishenina T.V., Soubiran C., Travaglio C., Busso M., 2002, *A&A*, 369,189
- Morton D.C., 2003, *ApJS*, 149, 205
- Nestor D., Rao S.M., Turnshek D.A., Vanden Berk D., 2003, *ApJ*, 595, L5
- Peroux C., McMahon R.G., Storrie-Lombardi L.J., Irwin M.J., 2003, *MNRAS*, 346, 1103
- Peroux C., Kulkarni V.P., Meiring J., Ferlet R., Khare P., Lauroesch J.T., Vladilo G., York D.G., 2006a, *A&A*, in press
- Peroux C., Meiring J., Kulkarni V.P., Ferlet R., Khare P., Lauroesch J.T., Vladilo G., York D.G., 2006b, *MNRAS*, to be submitted
- Pettini M., King D.L., Smith L.J., Huntstead R.W., 1997, *ApJ*, 478, 536
- Pettini M., Ellison S.L., Steidel C.C., Shapley A.E., Bowen, D.V., 2000, *ApJ*, 532, 65
- Prochaska J.X., Wolfe A.M., 1999, *ApJS*, 121, 369
- Prochaska J.X., Wolfe A.M., 2002, *ApJ*, 566, 68
- Rao S. M., Turnshek D. A., Nestor D. B., 2005, *ApJ*, in press (astro-ph/0509469)
- Rao S.M., Prochaska J.X., Howk C., Wolfe A.M., 2005, *AJ*, 129, 9
- Schulte-Ladbeck R.E., Knig B., Miller C.J., Hopkins A.M., Drozdovsky I.O., Turnshek D.A., Hopp U., 2005, *ApJ*, 625, L79
- Sembach K.R., Steidel C.C., Macke R.J., Meyer, R.J., 1995, *ApJ*, 445, L27
- Steidel C.C., 1998, *ApJ*, 492, 428
- Webster R.L., Francis P.J., Peterson B.A., Drinkwater M.J., Masci F.J., 1995, *Nature*, 375, 469
- Vidal-Madjar A., Laurent C., Bonnet R. M., York D. G., 1977, *ApJ*, 211, 91
- Vladilo G.,Centurin M., Bonifacio P., Howk J.C., 2001, *ApJ*, 557, 1007
- Vladilo G., Peroux C., 2005, *A&A*, 444, 461
- Welty D.E., Hobbs L.M., Lauroesch J.T., Morton D.C., Spitzer L., York D.G., 1999, *ApJS*, 124, 465
- Welty D.E., Hobbs L.M., York D.G., 1991, *ApJS*, 75, 425
- Wiess W.L., Fuhr J.R., Deters T.M., 1996 *J. Phys. Chem. Ref. Data*, Monograph 7
- Wild V., Hewett P.C., 2005, *MNRAS*, 361, L30
- Wild V., Hewett P.C., Pettini M., 2006, *MNRAS*, 367, 211
- Wolfe A. M., Lanzetta K. M., Foltz C. B., Chaffee F.H., 1995, *ApJ*, 454, 698
- Wolfe A.M., Gawiser E., Prochaska J.X., 2005, *ARAA* 43, 861,918
- York D.G., Khare P., Vanden Berk D., Kulkarni V.P., Crotts A.P.S., Lauroesch J.T., Richards G.T., et al., 2006, *MNRAS*, 367, 945